Journal of Materials Chemistry A

COMMUNICATION

View Article Online
View Journal | View Issue

Cite this: J. Mater. Chem. A, 2018, 6, 853

Received 26th October 2017
Accepted 20th December 2017

DOI: 10.1039/c7ta09466c

rsc.li/materials-a

3D printing of high performance cyanate ester thermoset polymers†

Swetha Chandrasekaran, Eric B. Duoss, Marcus A. Worsley and James P. Lewicki*

We report 3D printing of a 'pure' thermal cure cyanate ester for the fabrication of robust 3D printed structures through the formulation, tailoring and post processing of a custom 'ink' for Direct Ink Writing. Printed structures exhibit impressive thermo-oxidative stability, mechanical response.

Recently, additive manufacturing and 3D printing have emerged as one of the most promising routes for fabricating next generation, high performance composites. The main advantage of these techniques is the precise control that is enabled over the microstructure of the printed material, which results in novel or improved properties compared to parts made *via* traditional techniques.[1] One such 3D printing method, direct ink writing (DIW), has already been demonstrated as a promising route for the rapid fabrication of complex 3D structures with unique and enhanced properties for several different materials, ranging from graphene oxide suspensions to silicones, to thermoplastic and even carbon fiber filled polymers.[2–5] One of the main challenges for DIW is in the design and formulation of the feedstock 'inks' which must be rheologically tailored to form self-supporting filamentary layers required for DIW parts to be successful.[6,7] Polymer-based feedstocks used for DIW must meet certain requirements; such as shear thinning rheological behavior and long term mechanical stability. 3D printed parts formed from thermoplastics and UV curable resins have been successfully manufactured using DIW technology.[8–10] However, there are only limited examples of 3D printed composites and high T_g thermosets suitable for high performance structural applications; which are mechanically robust and capable of withstanding higher service temperatures for extended time periods than the current state of the art. Recently, Lewis *et al.*, demonstrated 3D printing of a thermoset epoxy resin with milled carbon-fibers exhibiting a 10-fold increase in the Young's modulus.[11] More recently, the authors have demonstrated the ability to 3D-print *via* a DIW method, high aspect ratio carbon fiber filled, high performance, thermal cure epoxy composites with orthotropic physical properties.[12] Such demonstrations highlight the possibilities, however, to date there has been no large-scale attempt to use DIW for the practical 3D printing of the extremely high T_g, thermally and mechanically robust specialist thermoset polymers such as cyanate ester resins. Herein, we report 3D printing of fine featured architectures of a new class of thermoset polymer for DIW – cyanate ester (CE) resins – which can be optimized to 3D print large scale structures with custom layouts and tuned thermomechanical response.

CE resins are a class of thermoset polymer networks that offer high thermal stability, low moisture absorption, high strength-to-weight ratios are widely used as composite matrices either directly or by blending it with epoxy for manufacturing structural components for applications in extreme environments.[13–15] Extensive research on the cure chemistry of CEs indicate that the cyclotrimerization reaction which forms a triazine ring is the primary polymerization process, which enhances the thermal stability of the resin system.[16,17] A schematic of the general polymerization process to form triazine ring is shown in Fig. 1.

The CE resin feedstock we have developed for our 3D printing process is a pure thermal cure system which remains glassy and rigid up to 280 °C and maintains its ultimate thermal oxidative stability up to 370 °C. The CE ink is rheologically tailored through the addition of silica nanoparticles to be both thixotropic and have a rapid, time dependent recovery on extrusion. Moreover, the inks can be thermally cured at elevated temperature (250 °C) to complete the polymerization process. Our CE-based inks also have low-moisture absorption behavior, show a high cure latency at room temperature and exhibit long pot-life (usually days) when stored in sealed containers.

To demonstrate the 3D printing of CE inks, we use DIW to print 3D structures of regular cubic geometries with well-defined unit cell size. The ink is loaded in a syringe barrel and extruded

Lawrence Livermore National Laboratory, 7000 East Avenue, Livermore, CA 94550, USA. E-mail: Lewicki1@llnl.gov

† Electronic supplementary information (ESI) available. See DOI: 10.1039/c7ta09466c

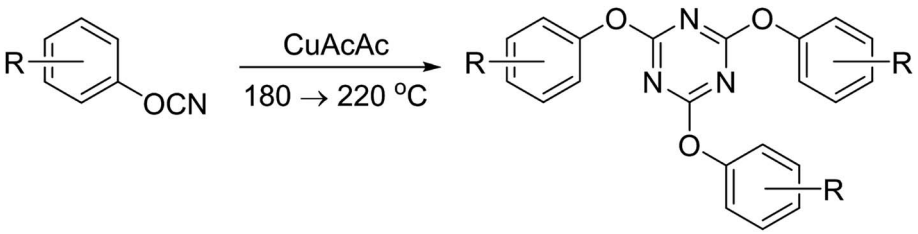

Fig. 1 Polymerization reaction of a cyanate ester resin to form a triazine ring network thermoset. Where 'R' may generally equal a secondary aryl group.

through a conical nozzle (250-micron inner diameter) by means of constant pressure (typically 25 psi). Our structures are thermally cured at 180 °C for 2 h and 220 °C for 2 h in air.

The viscosity measurements clearly show that addition of silica nanoparticles to the CE resin, and makes the resin have a shear thinning behavior (Fig. 2a) (in comparison with the newtonian behavior of the neat CE resin). Fig. 2a shows the as-printed CE structure in simple cubic morphology with a total of 8 layers with the center-to-center spacing of 800 μm between the filaments and for each layer the nozzle is moved up by 150 μm in the *z*-direction to maintain a good contact with successive layers. Due to the uncured nature of the resin and the intimate contact between layers we achieve molecular diffusion between layered strands, forming a contiguous structure (Fig. 2b). After printing, the parts are thermally cured in an oven and importantly, maintain their shape and geometry with the as-printed features (Fig. 2c). During printing, there are three major parameters (pressure applied for extrusion, writing speed and *z*-spacing) that need to be tuned to achieve well-defined filaments. Fig. 2d(a–c) shows one such example where the pressure and *z*-spacing was kept constant while the writing speed was varied to moderate feature size. In Fig. 2d–a, the center-to-center spacing between the filaments is increased from 0.25 mm to 1 mm and a continuous horizontal filament is printed on top. With a 5 mm s^{-1} writing speed, we see that the horizontal filament is no longer continuous at 1 mm spacing,

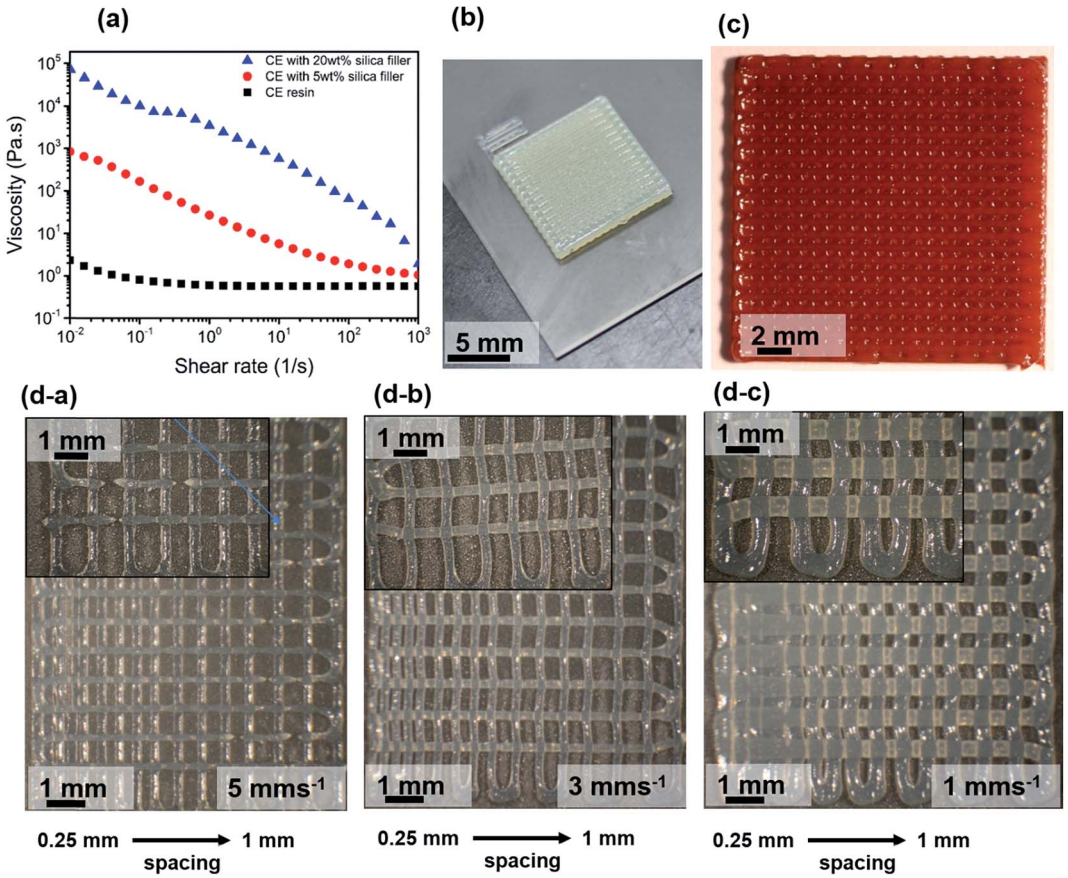

Fig. 2 (a) Viscosity of the rheologically tailored CE ink; (b) image of the as-printed structure on the substrate; (c) image of a fully cured 20 mm by 20 mm printed and (d(a–c)) as-printed CE with different varying ligament spacing at different writing speeds (5 mm s^{-1}, 3 mm s^{-1} and 1 mm s^{-1}).

however, this was not the case at 3 mm s^{-1} (Fig. 2d–b). Further decreasing the writing speed to 1 mm s^{-1} (Fig. 2d–c) yields thicker filaments and this can be avoided by varying the pressure applied for extrusion. Note that, for each printing in Fig. 2d, apart from the gradual increase in center-to-center spacing, the printing speed, and the *z*-spacing was kept constant. Thus, by optimizing the writing speed, applied pressure and by varying the *z*-spacing, it is possible to tailor the micro-architecture of 3D printed parts with larger spacing, while maintaining structural order.

The CE network formation is thermally driven in the presence of a transition metal catalyst.[17] The CE curing reaction occurs *via* a cyclotrimerization reaction by forming a stable six membered triazine ring.[18] The rate of the reaction is however, governed by the catalyst, cure schedule and driving the reaction to achieve full cross-linking density (100% network conversion) is non-trivial. Typically, transition metal salts are used to facilitate the cyclization reaction along with a co-catalyst which acts as a solvent for the metal ions and aids in completion of the reaction. We prepare the copper(II) acetyl acetonate metal salt catalyst, by dissolving in a minimal amount of chloroform and mixing with the resin. Initially, the samples were cured at 180 °C for 2 h and post-cured at 220 °C for 2 h in air. The effect of addition of different amounts of catalyst is studied through differential scanning calorimetry as shown in Fig. 3a. The exothermic peak observed at 400 °C arises from the onset of first stage thermal decomposition of the cyanate esters. The additional peaks observed between 205 °C and 350 °C are cure endotherms associated with incomplete formation of the cyanate esters network on primary cure. Upon increasing the amount of catalyst, we observe increased network degradation at elevated temperatures but no further increase in network conversion. Hence, an additional post cure at 250 °C for 12 h in nitrogen atmosphere was added to the initial cure conditions and the amount of catalyst added was maintained at 0.1 wt% of $Cu(acac)_2$. From Fig. 3b, it is evident that the additional peaks are no longer present which confirms the increase in conversion efficiency in the post-cured CE. Furthermore, a high final glass transition temperature of 280 °C was obtained for this thermally post-cured system. Fig. 3c, compares tensile properties of the resin cured with two different curing conditions, we observe that an additional post cure at 250 °C under nitrogen atmosphere increases the modulus by 9.5% and the strength by 29%. However, the elongation at break decreases due to the increased cross-linking density increasing the modulus of the network at the expense of tensile elongation.

Cyanate esters have been used in the recent years to produce carbon foams through direct pyrolysis at ambient pressures.[19,20] Here, we use a similar process on the 3D printed CE parts to convert them to refractory carbon composites by heating them to 1050 °C under inert atmosphere. When carbonized, the CE network converts to amorphous carbon which subsequently transforms to nano-crystallite graphite when the pyrolysis temperature is increased from 1050 °C to 2000 °C. This conversion has been confirmed through Raman analysis as shown in Fig. 4b. The conversion of CE to carbon foam occurs

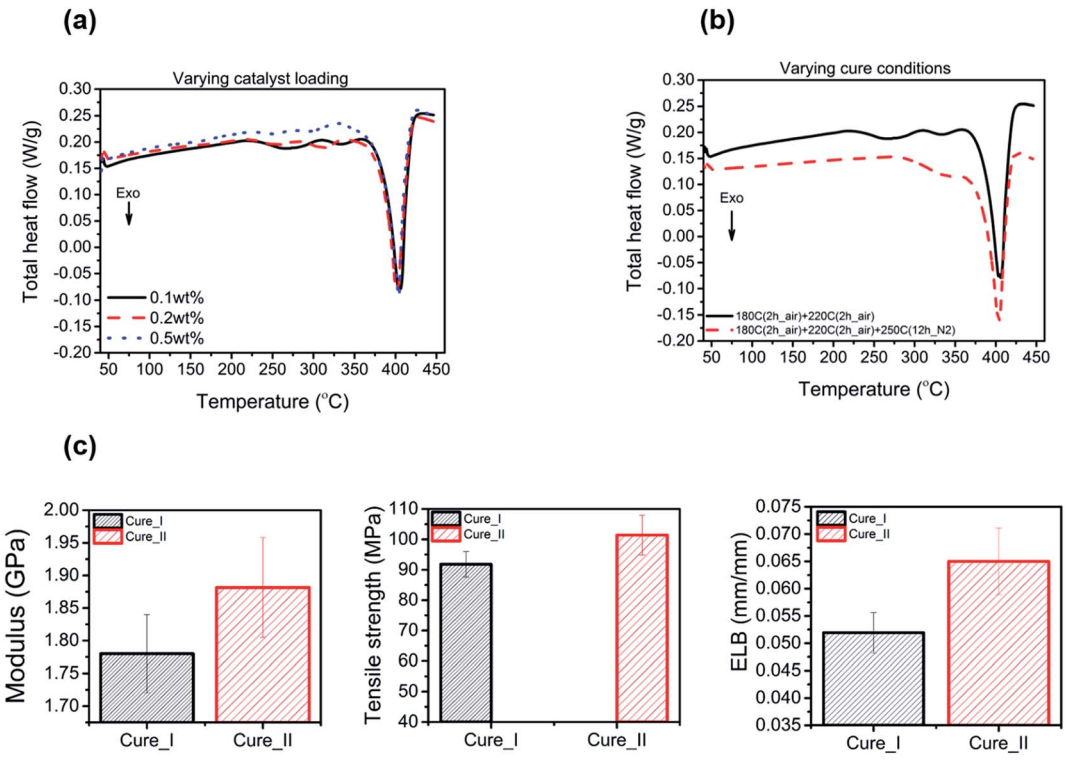

Fig. 3 Modulated DSC (first heating) of CE (a) with different amounts of catalyst and (b) with two different cure conditions at 0.1 wt% catalyst loading and (c) shows the modulus, tensile strength and elongation at break(ELB) for the two difference cure conditions.

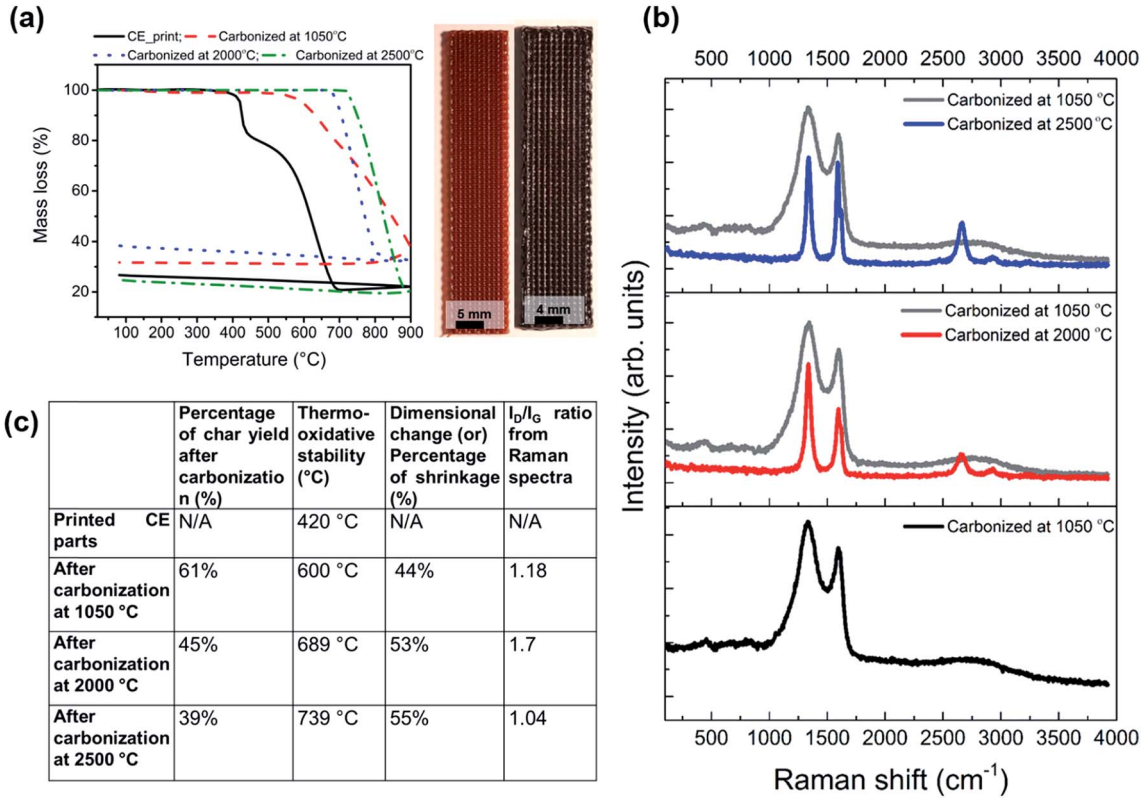

(c)

	Percentage of char yield after carbonization (%)	Thermo-oxidative stability (°C)	Dimensional change (or) Percentage of shrinkage (%)	I_D/I_G ratio from Raman spectra
Printed CE parts	N/A	420 °C	N/A	N/A
After carbonization at 1050 °C	61%	600 °C	44%	1.18
After carbonization at 2000 °C	45%	689 °C	53%	1.7
After carbonization at 2500 °C	39%	739 °C	55%	1.04

Fig. 4 Thermo-oxidative stability curves for (a) printed CE parts and printed CE carbonized at 1050 °C, 2000 °C and 2500 °C (on the right – photograph of samples before and after carbonization); (b) Raman spectra of printed CE carbonized at different temperatures with higher graphitization degree when carbonized at 2500 °C and (c) gives the char yield and I_D/I_G ratio from TGA and Raman data.

after 400–450 °C where the oxygen bond between the phenyl and triazine ring starts to degrade and the reductive conversion to a graphitic structure begins.[21] The thermal decomposition of the pure CE resin is studied through thermogravimetric analysis (TGA) where the sample is heated in air until 900 °C. Air atmosphere was chosen for TGA analysis as it is more relevant for practical applications. The samples were carbonized under nitrogen prior testing for thermo-oxidative stability.

There was no obvious change in mass of the fully cured, printed CE parts at temperatures below 400 °C suggesting excellent thermal stability under oxidative conditions (Fig. 4a). The printed CE samples undergo a two-step degradation process with the onset of mass loss (*i.e.*, temperature corresponding to a mass loss of 5%) occurring at 420 °C and continues to decrease to 86%, where, a second step in the curve is observed at 430 °C. Note, that the second degradation step is not due to the presence of silica particles added in the ink, and this was verified with CE base resin (see ESI†). By ~680 °C almost 80% of the resin has degraded leaving 20% of silica particles. In contrast, the carbonized printed CE parts show thermal stability until 600 °C. As expected, the higher the carbonization temperature, the more graphitized the carbon foams are and hence, they possess higher thermal stability. The carbonized 3D printed CE has a higher thermal oxidative stability compared to the as-printed CE at 600 °C (temperature corresponding to a mass loss of 5%) and a gradual degradation occurs until 870 °C where almost 63% of mass loss occurs. This is due to reaction of carbon with air and leaves the skeleton of silica particles in the printed structure.

It is evident from the TGA curve in Fig. 4a, that the silica added to the CE remains after carbonization. Note, that the char yield is calculated after removing the 20 wt% silica added to the CE resin. The relative density of the as printed CE part is 0.73 g cm^{-3} and when carbonized, it drops to 0.47 g cm^{-3}. Fig. 4c, summarizes the data from both and TGA and Raman analysis (Fig. 4b) of the printed CE parts before and after carbonization at different temperatures. Additionally, the carbonization procedure also makes the part electrically conductive and carbonized parts exhibit a conductivity of 5–6 S cm^{-1}. The modulus and hardness of the cured printed CE parts and carbonized CE parts were determined through nanoindentation of the printed parts. A five-fold increase in the modulus was observed for the carbonized printed CE parts with a modulus of 17 GPa compared to 3.3 GPa for printed CE. This enhanced mechanical robustness combined with improved thermal stability allowed the carbonized CE part to easily support a mass 100 times its own weight at elevated temperatures (see Graphical abstract).

Conclusions

We have developed a high temperature thermoset polymer based ink to 3D print thermal cure CE resin with excellent thermo-oxidative stability and high glass transition

temperature. The versatility of CE ink was demonstrated using DIW to build parts with features spanning several orders of magnitude. In addition to fabricating complex structures, the base material properties were optimized to withstand elevated temperatures up to 428 °C under thermo-oxidative conditions while maintaining its excellent mechanical properties. The printed CE resin when carbonized, maintains its printed structure and yields an even stiffer, more thermally robust refractory matrix with a five-fold increase in modulus. Such materials may be of great interest for advanced manufacturing applications.

Experimental section

Base resin and ink preparation

CE280 from Novoset® was used for the cyanate ester system and a metal salt copper(II) acetylacetonate ($Cu(acac)_2$) from Sigma Aldrich® was used as the curing agent/catalyst. An appropriate amount of catalyst was dissolved in a minimum amount of solvent (chloroform) and mixed in a Flackteck speed mixer for 1 minute at 3500 rpm. The resin mixture was degassed at room temperature for 2 h for solvent removal. The resin mixture was subjected to a thermal curing at 180 °C for 2 h in air followed by post curing at 220 °C for 2 h in air and 250 °C for 12 h in N_2, at a heating rate of 3°C min^{-1}. A thixotropic ink was prepared by mixing 20 wt% of Carbosil® TS530 silica to the resin mixture with a Flacktek speed mixer. The CE ink was degassed overnight at room temperature to remove air bubbles. The ink's rheological properties were measured using a stress controlled rheometer (AR 2000exTA). A plate–plate geometry with a gap of 500 μm was used to measure the viscosity at varying shear rates of the CE inks.

3D printing/direct ink writing (DIW)

Cyanate ester (CE) ink was loaded into a 3 ml syringe barrel (EFD) and centrifuged for 5 minutes at 4500 rpm to remove the air bubbles formed from loading of the ink. For direct ink writing, the syringe was attached by a luer-lock to a smooth-flow tapered nozzle whose inner diameter(d) is 250 μm. The ink was then extruded by means of an air powered fluid dispenser (Ultimus V, EFD) which provides an appropriate pressure (in the range of 55–70 psi) for writing. A simple cubic pattern was provided in a layer-by-layer fashion, where each layer was orthogonally oriented to the previous layer was selected for printing. The 3D micro-lattice was printed with different overall geometries and for each layer the nozzle moved up by 0.6d and the spacing between the rod-like filaments was 800 μm. The ink was printed on a glass slide coated with PTFE spray and was then subjected to thermal curing.

Thermal and mechanical characterization

The glass transition temperature of the cured CE resin with different catalyst loading and cure conditions was determined using a cryo-discovery series differential scanning calorimeter (DSC) from TA instruments. The samples were subjected to a temperature modulated heat–cool–heat cycle from 40 °C to 450 °C at 3 °C min^{-1} under a purge flow of helium. The mass of the samples was varied between 10–13 mg and the modulated time, amplitude was set to 40 s and 0.636 °C respectively during the temperature sweep. For Raman analysis, A Nicolet Almega XR dispersive micro-Raman spectrometer (Thermo Scientific) was used to determine the degree of graphitization from the intensity of D and G band. Spectra were collected at a wavelength of $\lambda = 633$ nm with a 50× objective, averaging over 25 five second scans.

For mechanical characterization, ASTM standard type V samples of the cured CE resin were prepared and tested using an Instron Instrument with a 2 kN load cell at a loading rate of 1 mm min^{-1}. The Young's modulus and hardness of the printed and carbonized parts were measured using indentation experiments following the Oliver-Pharr method. The measurement was conducted on a MTS Nanoindenter XP system equipped with a diamond Bekovich tip. Multiple unloading tests were run in each indent with 15 s loading, 10 s holding and 15 s unloading. The peak load increased linearly up to 500 mN to achieve a decent depth to minimize indentation size and surface roughness effects. Tip area calibration was carried out on a standard fused silica sample (Young's modulus – 72 GPa).

Carbonization

For carbonization, the cured CE printed structures were placed in a Lindberg/Blue M™ Mini-Mite™ tube furnace and heated up to 1050 °C from room temperature at a rate of 2 °C min^{-1} and held for 3 h. The samples were cooled down slowly to room temperature at 2 °C min^{-1}.

Conflicts of interest

There are no conflicts to declare.

Acknowledgements

This work was performed under the auspices of the U.S. Department of Energy by Lawrence Livermore National Laboratory under Contract DE-AC52-07NA27344, through LDRD award 15-ERD-030 with IM Release No. LLNL-JRNL-732246. The authors wish to acknowledge and thank Dr Jennifer N. Rodriguez for her assistance in tensile testing & Dr Jianchao Ye for his assistance in performing nano-indentation measurements. The authors also with to thank Novoset Inc. for their provision of cyanate ester resin samples.

References

1 Z. Quan, A. Wu, M. Keefe, X. Qin, J. Yu, J. Suhr, J.-H. Byun, B.-S. Kim and T.-W. Chou, *Mater. Today*, 2015, **18**, 503.
2 K. Sun, T.-S. Wei, B. Y. Ahn, J. Y. Seo, S. J. Dillon and J. A. Lewis, *Adv. Mater.*, 2013, **25**, 4539.
3 J. N. Rodriguez, C. Zhu, E. B. Duoss, T. S. Wilson, C. M. Spadaccini and J. P. Lewicki, *Sci. Rep.*, 2016, **6**, 27933.

4 C. Zhu, T. Y.-J. Han, E. B. Duoss, A. M. Golobic, J. D. Kuntz, C. M. Spadaccini and M. A. Worsley, *Nat. Commun.*, 2015, **6**, 6962.
5 Z. Quan, Z. Larimore, A. Wu, J. Yu, X. Qin, M. Mirotznik, J. Suhr, J.-H. Byun, Y. Oh and T.-W. Chou, *Compos. Sci. Technol.*, 2016, **126**, 139.
6 E. B. Duoss, T. H. Weisgraber, K. Hearon, C. Zhu, W. Small, T. R. Metz, J. J. Vericella, H. D. Barth, J. D. Kuntz, R. S. Maxwell, C. M. Spadaccini and T. S. Wilson, *Adv. Funct. Mater.*, 2014, **24**, 4905.
7 J. A. Lewis, *Adv. Funct. Mater.*, 2006, **16**, 2193.
8 H. L. Tekinalp, V. Kunc, G. M. Velez-Garcia, C. E. Duty, L. J. Love, A. K. Naskar, C. A. Blue and S. Ozcan, *Compos. Sci. Technol.*, 2014, **105**, 144.
9 R. Matsuzaki, M. Ueda, M. Namiki, T.-K. Jeong, H. Asahara, K. Horiguchi, T. Nakamura, A. Todoroki and Y. Hirano, *Sci. Rep.*, 2016, **6**, 23058.
10 M. Chapiro, *Reinf. Plast.*, 2016, **60**, 372.
11 B. G. Compton and J. A. Lewis, *Adv. Mater.*, 2014, **26**, 5930.
12 J. P. Lewicki, J. N. Rodriguez, C. Zhu, M. A. Worsley, A. S. Wu, Y. Kanarska, J. D. Horn, E. B. Duoss, J. M. Ortega, W. Elmer, R. Hensleigh, R. A. Fellini and M. J. King, *Sci. Rep.*, 2017, **7**, 43401.
13 J. Ajaja and F. Barthelat, *Composites, Part B*, 2016, **90**, 523.
14 A. Toldy, Á. Szlancsik and B. Szolnoki, *Polym. Degrad. Stab.*, 2016, **128**, 29.
15 P. Ren, G. Liang and Z. Zhang, *Polym. Compos.*, 2006, **27**, 402.
16 A. Osei-Owusu, G. C. Martin and J. T. Gotro, *Polym. Eng. Sci.*, 1992, **32**, 535.
17 *Chemistry and Technology of Cyanate Ester Resins*, ed. I. Hamerton, Springer Science, 1994.
18 I. Harismendy, C. M. Gómez, M. D. Río and I. Mondragon, *Polym. Int.*, 2000, **49**, 735.
19 T. Chen, Q. Lin, L. Xiong, Q. Lü and C. Fang, *J. Anal. Appl. Pyrolysis*, 2015, **113**, 539.
20 Q. Lin, B. Luo, L. Qu, C. Fang and Z. Chen, *J. Anal. Appl. Pyrolysis*, 2013, **104**, 714.
21 U. Szeluga, B. Kumanek, S. Pusz and S. Czajkowska, *J. Therm. Anal. Calorim.*, 2015, **122**, 271.

